Journal of Membrane Science 685 (2023) 121941

Contents lists available at ScienceDirect

Journal of Membrane Science

journal homepage: www.elsevier.com/locate/memsci

Metal-Organic-Framework-based nanofiltration membranes for selective multi-cationic recovery from seawater and brines

C. Morgante [a], X. Ma [b], X. Chen [b], D. Wang [c], V. Boffa [b,*], V. Stathopoulos [d], J. Lopez [e,f], J.L. Cortina [e,f], A. Cipollina [a], A. Tamburini [a], G. Micale [a]

[a] Dipartimento di Ingegneria, Università degli Studi di Palermo - viale delle Scienze Ed.6, 90128, Palermo, Italy
[b] Department of Chemistry and Bioscience, Aalborg University, Fredrik Bajers vej 7H, 9220, Aalborg, Denmark
[c] Department of Physics and Nanotechnology, Aalborg University, Skjernvej 4, 9220, Aalborg, Denmark
[d] Department of Agricultural Development, Agrofood and Management of Natural Resource, National and Kapodistrian University of Athens, Psachna Campus, 34400, Evia, Greece
[e] Chemical Engineering Department, Escola d'Enginyeria de Barcelona Est (EEBE), Universitat Politècnica de Catalunya (UPC)-Barcelona TECH, Campus Diagonal-Besòs, 08930, Barcelona, Spain
[f] Barcelona Research Center for Multiscale Science and Engineering, Campus Diagonal-Besòs, 08930, Barcelona, Spain

ARTICLE INFO

Keywords:
Mineral recovery
Brine valorization
Critical raw materials
Metal-organic-framework
Zinc oxide

ABSTRACT

Nanofiltration (NF) is gaining a role of increasing importance in Zero Liquid Discharge (ZLD)/Minimal Liquid Discharge (MLD) systems, enhancing the efficiency of downstream technologies to recover valuable minerals from seawater and brines. However, often the purity of the recovered minerals does not meet market specifications, making ZLD/MLD currently economically unfeasible. To such end, in this study, a novel positively charged NF membrane was developed to enhance magnesium and calcium selectivity. The membrane comprised: (i) an ultrafiltration substrate and (ii) an active layer that incorporated NH_2-MIL-101(Al) and ZnO nanoparticles in a chitosan matrix. The influence of different loadings of NH_2-MIL-101(Al) and ZnO on membrane structure, selectivity and water permeability was investigated. Initial filtration tests with single-salt solutions at 1000 ppm (NaCl, Na_2SO_4, $MgCl_2$, $CaCl_2$) showed that the membrane with 35%wt of ZnO presented the highest rejections of $MgCl_2$ (90.10%) and $CaCl_2$ (86.49%). Selectivity towards $MgCl_2$ and $CaCl_2$ was higher than those of commercial membranes (NF90 and NF270) and the positively charged membranes introduced in recent literature. The novel synthesized membrane in this work was also tested with synthetic seawater and brine at a *trans*-membrane pressure of 30 bar. Results highlighted the intriguing competitiveness of the novel membrane in terms of magnesium and calcium selectivity with NF90 and NF270 within the field of both seawater and brine valorization.

1. Introduction

In the last decades, the lack of primary resources witnessed by the European Union (EU) has resulted in the call to define 30 Critical Raw Materials (CRMs) [1]: elements of both economic importance and high-risk supply [2], such as magnesium. Several action plans have been brought to life to recover CRMs from unconventional sources. Such plans focus on the development of sustainable and low carbon-emission methods, thus solving both economic and environmental issues related to traditional land-mining [3]. Among the unconventional sources, worldwide seawater contains approximately 5×10^{16} tonnes of salts: a quantity estimated to be much more than the minerals available from all the land-based mines combined [4]. Many elements are present in seawater (i.e. magnesium, calcium, etc.) although most of them have very low concentrations [5,6]. A further unconventional source that has captured greater interest recently is desalination waste brine [7]. The increasing volume of waste brine discharged to the environment [8] and the higher concentration of minerals present in brine compared to seawater [4], have led to exploit such waste as a promising alternative source for minerals recovery, implementing the concept of circular economy [9]. To such an end, different Zero Liquid Discharge (ZLD)/Minimal Liquid Discharge (MLD) solutions have been proposed [10]. ZLD/MLD systems consist of an integration of membrane-based and thermal-based technologies to recover valuable resources (water,

* Corresponding author.
E-mail address: vb@bio.aau.dk (V. Boffa).

https://doi.org/10.1016/j.memsci.2023.121941
Received 3 May 2023; Received in revised form 10 July 2023; Accepted 16 July 2023
Available online 17 July 2023

minerals and/or energy), reducing the volume of waste discharged to the aquatic ecosystem [11]. Nanofiltration (NF) is a technology that is most often present in such integrated schemes and is of great importance to the performances of the entire ZLD/MLD systems. NF is a pressure-driven membrane process with higher selectivity when compared to reverse osmosis (RO) [12]. NF membranes present a pore size in the range 0.5 nm–2 nm [13] and through the combined effect of steric exclusion, Donnan exclusion and dielectric exclusion, such membranes present high selectivity towards multi-valent ions [14]. Attractive features such as low operating pressure, low energy consumption and high separation selectivity [15], have brought NF to be chosen as a pre-treatment step in most ZLD/MLD schemes.

Figueira et al. [16] highlighted the relevance of NF as a pre-treatment step for brine valorization in the EU Horizon 2020 project Sea4Value [17]. Three different commercial NF membranes (NF270, Fortilife XC-N, PRO-XS2) were tested at lab-scale. Results showed that PRO-XS2 presented the highest selectivity towards all multivalent ions. Reig et al. [18] treated seawater reverse osmosis brine via NF at a pilot scale, employing NF270 at 20 bar. The pilot plant served as a pre-treatment step to an electrodialysis with a bipolar membrane unit for chemical production. The NF retentate presented enrichment factors of 3.2 and 2.5 for magnesium and calcium, respectively. Ali et al. [19] proposed NF as desalination brine pre-treatment for a series of RO stages in a ZLD configuration. The commercial membrane NF-2012-250 presented rejections of 98%, 91%, 54% and 46% for Mg^{2+}, Ca^{2+}, Cl^{-} and Na^{+}, respectively. Morgante et al. [20] investigated the influence of NF as a pre-treatment step on the recovery and purity of sodium chloride recovered from brine. The NF step was part of a novel MLD scheme proposed in the EU H2020 ZERO BRINE project [21]. Simulation results revealed that the set of ion membrane rejections of NF270 had to be increased by a correction factor of 0.7 to achieve a food-grade salt from a downstream thermal crystallizer. Du et al. [22] modeled a process chain for sodium hydroxide NaOH production from seawater desalination brine employing NF as pre-treatment, separating monovalent from multivalent elements in the permeate and concentrate respectively, for a further recovery process. All in all, it is very much explicit how in literature, most works based on NF in ZLD/MLD schemes directly took into account commercial polymeric membranes.

Commercial polymeric NF membranes, due to their fabrication material, are generally neutral or exhibit a negative surface charge when employed in seawater treatment or similar applications [23–25]. Only when employed in highly acidic environments, do they actually present a positive surface charge (i.e. pH < 4). It has been reported in literature that a negative surface charge is not suitable for certain applications, such as salt recovery from textile effluents and heavy metal recovery from industrial wastewater [23], where high multivalent cationic selectivity is required. This is also the case for high valuable mineral recovery from seawater and brines. As mentioned previously, NF is frequently employed as a pre-treatment step in ZLD/MLD systems, providing concentrated feed streams for its downstream technologies [20]. However, with positively charged NF membranes, the possible production of an NF retentate stream highly rich in magnesium and calcium would offer several advantages. Among which, (i) higher purity products would be achieved when the retentate undergoes a downstream crystallization process and (ii) a reduction of the purification technologies would lead to lower capital and operating costs of ZLD/MLD systems. In the past decade, different attempts have been made and proposed in literature to synthesize positively charged NF membranes. An overview of selectivity and permeation performances of such membranes is presented in Table 1.

None of the membranes in literature (reported in Table 1) was (i) designed and applied for mineral recovery from seawater/brine and (ii) characterized by a sufficiently high multi-cationic selectivity, presenting most often significant membrane rejection for sodium chloride or sulfate-based salts. To such an end, the current study proposes a novel positively-charged NF membrane, purposely synthesized to selectively recover calcium and the high valuable (and critical according to EU) magnesium from seawater and waste brines in an MLD/ZLD context. More specifically, the novel membrane comprised: (i) a highly permeable polysulfone ultrafiltration substrate and (ii) an active layer consisting of a positively charged metal-organic-framework (MOF) and a highly hydrophilic metal-oxide nanofiller within a chitosan matrix. Bearing in mind the specific target application, one particular MOF, namely NH_2-MIL-101(Al), was used in the current study. Such MOF derives from the MIL-101 family, vastly studied and employed for gas separation applications due to their high specific surface area and microporosity as reported previously [39]. Reasons for using NH_2-MIL-101(Al) here are further related to the intent of both providing a good mixing with the other components of the active layer and increasing the positive surface charge [38] of the NF membrane. More precisely, the highly charged metal centre with cationic functional groups (i.e., amino groups) of NH_2-MIL-101(Al) guarantees a high positive surface charge in a wide pH range unlike other MOFs previously introduced in literature for nanofiltration membrane fabrication [40–42]. Chitosan essentially acted as a binder between the active layer and substrate and attracted the authors of the current study, being a low-cost, biodegradable and anti-microbial material [43]. Moreover, a nanofiller was used to improve the separation performances of the new membrane. Indeed, the incorporation of a range of dense (non-porous) nanofillers, such as nanoparticles consisting of TiO_2, amorphous SiO_2, silver, and carbon quantum dots (CQDs), have been recently proposed in literature as a strategy to enhance the permeability-selectivity trade-off of polymeric NF and RO membranes [44]. Despite their dense structure, at certain loadings these nanofillers can potentially promote water permeability by increasing the free volume in the active layer matrix [45,46] and can lend additional functionalities to the membrane like

Table 1
Selectivities and water permeabilities of novel positively charged thin film NF membranes in literature.

Ref.	Substrate/Active layer	Permeability [L m^{-2} h^{-1} bar^{-1}]	Feed Concentration	Operating Pressure [bar]	Rejection [%]			
					$MgCl_2$	$CaCl_2$	NaCl	Na_2SO_4
[26]	PES/PEI + TMC	3.06	500 mg L^{-1}	8	95	–	80	75
[27]	PAN/PEI + ECH	1.67	2000 mg L^{-1}	5	93	–	60	–
[28]	PSF/pDA	13.90	0.01 mol L^{-1}	6	65	70	25	30
[29]	PAN/catechol + PEI	2.92	2000 mg L^{-1}	5	85	–	48	55
[30]	PSF/DADMAC	12.00	1000 mg L^{-1}	5	90	92	50	15
[31]	PES/PEI + PIP	5.20	2000 mg L^{-1}	4	97	98	49	69
[32]	PVC/PIP + TMC	8.70	1000 mg L^{-1}	3.5	99	98	–	96
[33]	PES/PEI + TMC	17.00	1000 mg L^{-1}	5	95	–	40	55
[34]	PSF/DMC	7.50	1000 mg L^{-1}	5	92	–	62	22
[35]	PAN/HACC	1.06	1000 mg L^{-1}	5	95	95	28	60
[36]	PEKC/PAMAM + TMC	10.00	1000 mg L^{-1}	5	96	–	73	58
[37]	PSF/PDMAEMA	1.00	1000 mg L^{-1}	6	98	–	78	66
[38]	PSF/Chitosan + MOF	3.50	1000 mg L^{-1}	5	93	86	30	25

antifouling properties [47,48]. In the present work, the authors selected ZnO as a nanofiller for the proposed composite membranes due (i) its positive charge in aqueous solutions within a wide pH range, and (ii) hydrophilic properties [49,50]. These features give the potential to increase Mg^{2+} rejection without compromising the permeability of the membrane. Additionally, ZnO nanoparticles are inexpensive when compared to other nanofillers and present such a low toxicity that they have been proposed as active components in food packaging [51,52]. The new NF membrane was optimized via different loading of ZnO/NH_2-MIL-101(Al) within the active layer. Filtration tests at lab-scale were performed with both single salt solutions and synthetic seawater and brine, highlighting superior selectivity towards magnesium and calcium when compared to the commercial and lab-made NF membranes reported in literature.

2. Experimental

2.1. Materials

2-aminoterephthalic acid (Sigma-Aldrich, purity = 99%), $AlCl_3{\cdot}6H_2O$ (Alfa Aesar, 98%) and dimethylformamide DMF (VWR chemicals, HPLC grade, >99.9%) were employed for the synthesis of the MOF nanocrystals. Acetone and methanol (HPLC grade, ≥99.9%) used for washing MOF were supplied by VWR Chemicals. NaOH pellets were procured from VWR chemicals. Chitosan (Aldrich, medium molecular weight), ZnO nanopowder (Sigma Aldrich Merck, particle size <100 nm) and acetic acid (Fisher Chemical, >99.7%) were employed for the synthesis of the selective active layer of the NF membranes. NaCl (Chemsolute, 99%), Na_2SO_4 (Sigma Aldrich, >99.0%), $MgCl_2{\cdot}6H_2O$ (PanReac AppliChem, pharma grade) and $CaCl_2{\cdot}2H_2O$ (VWR chemicals, pharma grade) were used to characterize the salt rejection of the NF membranes introduced in this work. Deionized water (resistivity >18 MΩ) was employed throughout MOF syntheses, membrane fabrication, and the preparation of salt solutions for all the filtration tests. Furthermore, two commercial NF membranes (models: NF90 and NF270) were purchased from Dupont for filtration tests and comparison purposes.

2.2. MOF synthesis

The synthesis of NH_2-MIL-101(Al) was carried out by means of the solvothermal method [53]. According to such procedure, 0.51 g of $AlCl_3{\cdot}6H_2O$ and 0.56 g of 2-aminoterephthalic acid were physically mixed in 30 mL of DMF and stirred for 30 min. The solution was then placed in a Teflon-lined autoclave and heated in a static oven (Memmert UF 30) for 72 h at 130°C. Subsequently, once cooled to room temperature, the resulting yellow powder was vacuum filtered and washed 3 times with acetone. An activation process of the remaining powder was performed by refluxing the MOF with boiling methanol overnight to remove residual organic species still trapped within the pores. The MOF was then dried in a static oven for 16 h at 200°C.

2.3. Membrane fabrication

An ultrafiltration polysulfone PSF membrane with a molecular weight cut-off of 25,000Da was purchased by Alfa Laval (model: DSS-GR60PP) and used as the substrate of the novel NF membranes. Before coating, the substrate was pre-treated via immersion in a 1 M NaOH solution for 1 h. Reasons for this were to (i) "activate" the substrate surface facilitating the bonding between substrate and active layer and (ii) remove the glycerine present in the pores of the commercial UF membrane. Subsequently, the substrate was then rinsed 3 times with deionized water. Once the substrate pre-treatment was completed, the NF membranes were prepared by solvent-casting the coating solution on the substrate via a spiral bar-coater (purchased from TQC) with a thickness of 50 μm. The dispersions for the coating of the membrane active layers were prepared as follows: chitosan was dissolved (20%wt) in an aqueous acetic acid 2%wt solution. Then, ZnO nanopowder and the MOF were gradually added to the chitosan solution under stirring conditions. Active layers with different compositions were prepared, as reported in Table 2, to subsequently investigate the effect of the ZnO and MOF loadings on the structure, selectivity and permeability of the membranes. The active layer dispersions were magnetically stirred for 24 to guarantee a homogenous coating. They were then subjected to an ultrasonic bath for 30 min to remove all gas that could compromise the coating procedure. The coated membranes were finally set to dry in a static oven at 80°C for 2 h to complete the solvent evaporation process and consolidate the active layer.

2.4. Membrane characterization

X-ray diffraction XRD analyses were carried out to confirm the crystallographic structure of the MOF and ZnO over an Empyrean diffractometer (Malvern Panalytical) equipped with a monochromator Cu Kα radiation (1.5406 Å). The X'Pert HighScore Plus (Malvern Panalytical) and the references provided with the software were used to analyse the diffractograms crystal phases (i.e., ZnO hexagonal and cubic, ZnS hexagonal, and MIL-53) at the exception of the peaks corresponding to the MIL-101 phase, which were determined by comparison with the relevant literature [53]. The size distribution and the ζ-potential of nanopoweder and coating dispersions were investigated by dynamic light scattering (DLS) on a Zetasizer Nano ZS (Malvern Instruments). Particle size measurements were performed on MOF and ZnO dispersion (0.1 mg L^{-1}). In the case of the ζ-potential measurements, the coating dispersions were diluted 1:250 in deionized water and the pH was corrected accordingly via addition of NaOH or HCl. For each membrane sample, the zeta-potential was measured within the pH range 3–12 and each sample at a specific pH value was analyzed three times, considering a final average value. Attenuated total reflectance - Fourier-transform infrared ATR-FTIR spectroscopy (Bruker Tensor II) analyses were performed to verify that the active layer of the NF membrane presented the moieties characteristics of Chitosan, ZnO and the MOF (NH_2-MIL-101 (Al), Each ATR-FTIR spectrum was collected by the accumulation of 30 scans at a resolution of 4 cm^{-1} covering a wavenumber from 4000 to 350 cm^{-1}. The morphologies of the MOF powder and of the coated membranes were analyzed via field emission scanning electron microscopy (FE-SEM) (Zeiss 1540XB). Gold was sprayed on the sample surface before the measurements and images, with a magnification of 180,000, were taken. The FE-SEM were furthermore accompanied by Energy-dispersive X-ray (EDX) spectroscopy measurements to better identify the active layer. The concentration of the relevant elements (C, S, O, Zn, Al) was determined. The effect of the presence of ZnO on the surface hydrophilicity of the NF membrane was investigated via the use of a contact angle meter (Biolin Scientific - Attention Theta Lite). Prior to the contact angle measurements, the membrane samples were air dried at room temperature. The measurements analyzed a sessile drop of deionized water with a diameter of 5 mm. Parameters of the contact angle camera were the following: Exposure = 1400, Gain = 1110, Gamma = 2793. Three different readings were taken per sample and, for each reading, 40 images were taken per second for a total of 30 s. For each membrane sample an average value of the measurements was considered.

Table 2
Composition of the membranes fabricated and tested in this work.

Name	Weight composition (w/w)		
	ZnO [%]	NH_2-MIL-101(Al) [%]	Chitosan [%]
CMZ-0	0	80	20
CMZ-20	20	60	20
CMZ-35	35	45	20
CMZ-60	60	20	20
CMZ-80	80	0	20

2.5. Filtration tests

The separation performances of the NF membranes were evaluated in terms of salt rejection and permeability. Experimental tests were carried out at 5 bar and room temperature, employing the cross-flow experimental set-up schematically illustrated in Fig. 1. 3 L solution was fed via a dosing pump (Wanner Hydracell dosing pump, model G03) to a flat sheet stainless steel NF module (Sterlitech). The flow rate of the feed solution entering the module was monitored via a flow meter (Siemens, Sitrans F M Magflo MAG5000). The permeation active area of the NF module was 33.4 cm^2. During the tests, the NF retentate was circulated by means of a cross-flow rotary lobe pump (Hilge, Grundos, model Novalobe 10). A part was recycled back to the NF module whereas the remaining retentate was sent back to the feed solution. The transmembrane pressure was monitored via two pressure transmitters (Danfoss, model MBS 4010) placed on the feed pipeline and the retentate pipeline and the operating pressure was regulated by means of a needle valve positioned on the latter pipeline. The permeate was collected in a beaker placed on an analytical scale (Kern, PCB). By means of a simple program implemented in Matlab software, the permeate mass collected over a certain period of time, monitored by the scale, was recorded and computed into the NF transmembrane permeability according to equation (1).

$$\varnothing = \frac{V}{A \times t \times P} \tag{1}$$

Where Φ is the permeability of the NF membrane [L m^{-2} h^{-1} bar^{-1}], V is the volume of NF permeate [L], A is the membrane active area [m^2], t is the operation time [h] and P is the relative transmembrane pressure during the experiment [bar].

Prior to each filtration test, the membrane under investigation was pressurized at 5 bar with deionized water for 1 h. This allowed to guarantee a stabilized water flux during the experimental tests and also to remove possible traces of glycerine still present in the substrate that could compromise the conductivity of the NF permeate. The selectivity of each NF membrane was investigated by testing four different single salt solutions at a concentration of 1000 mg L^{-1}: NaCl, Na_2SO_4, $MgCl_2$ and $CaCl_2$. The conductivity and pH of the feed and the permeate solutions were monitored via a pH/conductivity meter (Mettler Toledo, SevenCompactDuo). The salt rejection was evaluated as:

$$R(\%) = \left(1 - \frac{C_p}{C_f}\right) = 100 \tag{2}$$

where $R(\%)$ single salt rejection, C_f the conductivity of the feed solution [mS cm^{-1}] and C_p the conductivity of the permeate solution [mS cm^{-1}]. It should be noted that equation (2) was employed only when dealing with pure single salt solutions (due to the linear relationship between concentration and conductivity). For the calculation of ion rejection with synthetic seawater and brine feed solutions, equation (2) was expressed in terms of ion concentration instead of conductivity. Furthermore, it is worth mentioning that the volume of permeate solution collected was chosen to be equal to 50 mL (negligible compared to the initial feed solution volume equal to 3 L). Due to this large difference of volume, the recycling strategy of the retentate solution did not concentrate the feed solution during the filtration tests. All experiments were repeated at least twice, and average values of salt rejection and permeability were reported in Section 3.3. Subsequent to the filtration tests with single salt solutions, the best performing NF membrane was selected and tested with synthetic solutions of seawater and RO desalination brine. The composition of the major ions of both solutions is reported in Table 3.

Experimental tests with synthetic solutions were performed at 30 bar (typical operating pressure at industrial scale). Samples of feed and permeate were taken and analyzed via Ionic Chromatography. Ion selectivity of the novel NF membrane was calculated according to equation (3):

Table 3
Major ions concentration of synthetic seawater and RO desalination brine.

Ion	Concentration [mg L^{-1}]	
	Seawater	RO Desalination Brine[a]
Na^+	12500	22727
Mg^{2+}	1450	2636
Ca^{2+}	450	818
Cl^-	22100	40182
SO_4^{2-}	3410	6200

[a] A desalination plant with a typical permeate recovery of 45% was taken into consideration for the composition of the desalination brine.

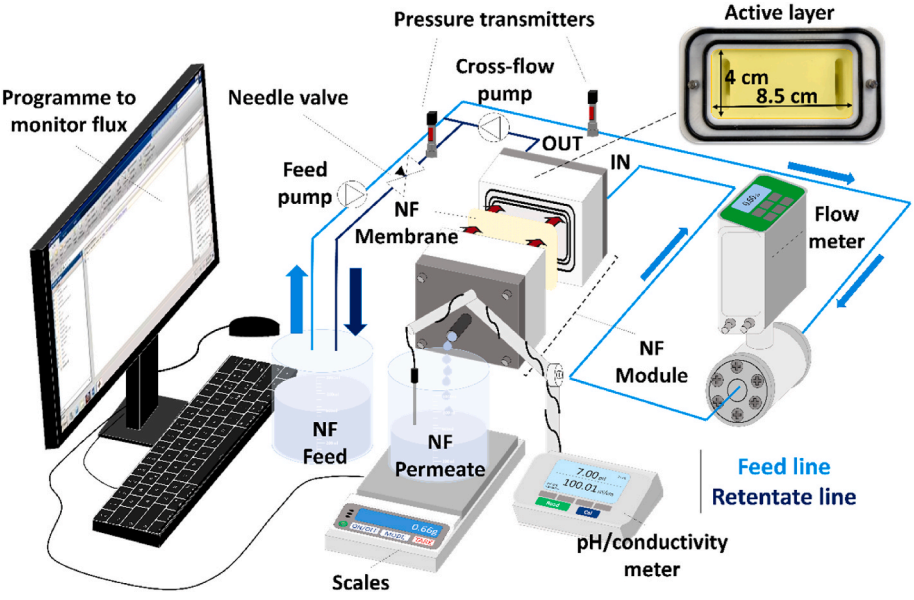

Fig. 1. Conceptual scheme and main components of the flat-sheet nanofiltration experimental set-up used in this study.

$$IS_{\frac{ion1}{ion2}} = \left(1 - \frac{R_{ion2}}{R_{ion1}}\right) \quad (3)$$

Where *IS* is the ion selectivity between the rejections *R* of two ions ion_1 and ion_2. When the rejections of two ions are equal *IS* is equal to 0 (no selectivity). On the contrary, when the two rejections assume values of 100% and 0% respectively, *IS* is equal to 1. In this study, the *IS* of the novel NF membrane was compared to that of two commercial NF membranes (NF90, NF270) tested at the same operating conditions.

3. Results and discussion

3.1. Characterization of the membrane materials

3.1.1. MOF and ZnO nanoparticles

Structure and composition of the starting nanomaterials, namely MOF were studied by XRD analysis. The diffractogram reported in Fig. 2a shows the characteristic reflections of MIL-101 phase with the main peaks at 2θ values of 8.6°, 9.3°, 15.1°, and 18.2° in good agreement with [54] and references therein. The broad peaks are consonant with ~15 nm large crystallites [55]. Moreover, the peaks at 12.3°, 17.5°, and 25.1° indicate the presence of the phase MIL-53, as impurity. Nevertheless, the potential residual peaks corresponding to the reagents used in the MOF synthesis were not detected, suggesting their full conversion in MOF nanoparticles. As far as ZnO was concerned, such nanopowder was purchased, unlike the MOF. As can be observed in Fig. 2b, the diffractogram of the ZnO nanopowder presented narrow peaks, corresponding to a highly ordered crystalline material. From the analysis of the reflection data, it was possible to determine that this ZnO nanopowder consisted for more than 97 wt% of wurtzite (hexagonal phase), while the major impurities were determined to be the cubic ZnO and cubic ZnS phases.

The dispersibility of nanoparticles in a solvent (typically water) is an essential feature for the deposition of thin film filtration layers, as required for the fabrication of thin film NF membranes. As shown in Fig. 2c, a narrow size distribution was measured for the water dispersion of the ZnO nanopowder with an average hydrodynamic diameter smaller than 90 nm, which is consistent with the product specification (i.e., particle size <100 nm). Thus, DLS analysis indicates that ZnO nanoparticles can be easily dispersed in water with no need for chemical additives, which is consistent with the high hydrophilicity and surface charge of this material [56,57]. The MOF powder also yielded a stable dispersion in water, but its particle size ranged between 300 and 450 nm (Fig. 2c), indicating aggregation of the MOF in colloids with size much larger than the single crystallites.

The SEM micrograph in Fig. 3a confirmed the MOF powder is homogenous. The high magnification image in the insert shows that this material consisted of small crystallites aggregated in secondary particles reaching dimensions of a few hundred nanometres and with morphology similar to that reported for NH_2-MIL-101(Al) in literature [58]. Moreover, a specific surface area of 501 m^2 g^{-1} was calculated from the low-temperature (77 K) nitrogen adsorption/desorption isotherms in Fig. 3b, which was also in agreement with previous values reported in literature [38] and thus provided a further indication that the MOF was successfully synthesized. More precisely, a highly microporous product was achieved as indicated by the large nitrogen uptake at low relative pressures. The high porosity in the micropore range was among the features, in reason of which the MOF was selected as the main component of the separation layer in this work, as it was a requirement to achieve a thin film NF membrane which combines high ion selectivity and high-water permeability.

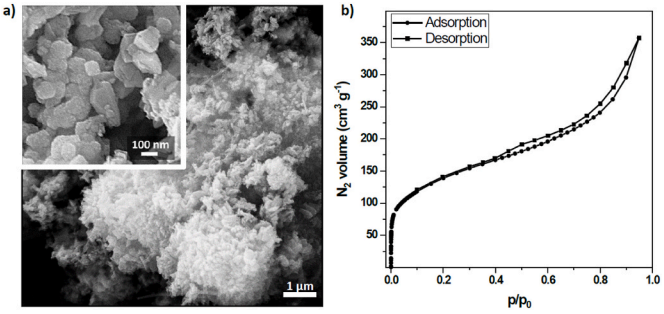

Fig. 3. NH_2-MIL-101(Al) powder: (a) low-magnification and high-magnification (in the insert) SEM micrographs, and (b) nitrogen adsorption/desorption isotherms (77 K).

3.1.2. CMZ nanocomposites

Fig. 4 allows comparing the ATR-FTIR spectra of the membrane components, namely chitosan, MOF, and ZnO, to the one of the CMZ-35 nanocomposite, which was used as membrane active layer. The main purpose of this comparison was to observe whether the single components preserved their structures when combined in the membrane active layer. The ATR-FTIR spectrum of commercial chitosan presents the characteristic peaks of this material: the stretching modes of –OH and $–NH_2$ groups within the polysaccharide structure in the range 3000–3500 cm^{-1}, the C–H stretching at 2870 cm^{-1}, and the characteristic signals lying at 1724, 1447, and 1000 cm^{-1}, within the footprint region of the chitosan and characteristic of the O–C–OH, $–CH_2$, and –C–O–C– groups, respectively. The spectrum of NH_2-MIL-101(Al) was in good agreement with those of the same MOF reported previously in literature [54,59,60], confirming the success of the MOF synthesis in this work. The spectrum presented a peak at 3640 cm^{-1}, which corresponded to

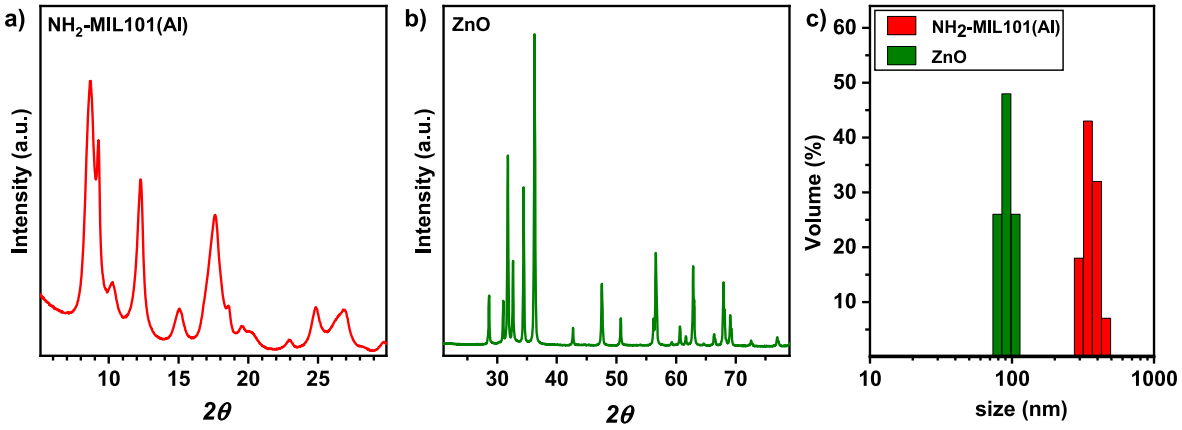

Fig. 2. a) XRD analysis of NH_2-MIL-101(Al); b) XRD analysis of ZnO; c) Size distributions of NH_2-MIL-101(Al) and ZnO nanoparticles dispersed in demineralized water as measured by DLS analysis.

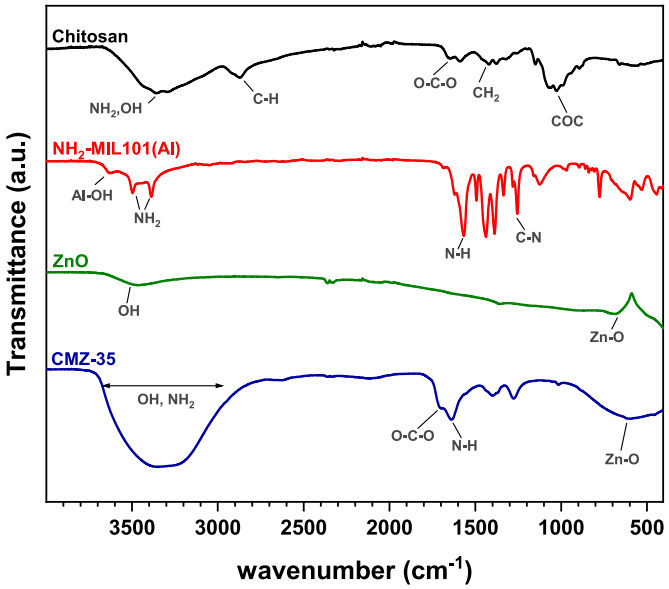

Fig. 4. FTIR analysis of chitosan, NH_2-MIL101(Al), ZnO, and CMZ-35 nanocomposite.

Al–OH groups and two distinctive peaks in the region between 3385 and 3495 cm^{-1}, which could be associated with the symmetrical and asymmetrical $–NH_2$ stretching, respectively. The peaks detected at 1565 and 1340 cm^{-1} were indicative of the N–H and C–N moieties, respectively. The spectrum of the ZnO nanopowder showed two peaks: one at high frequency (3500 cm^{-1}) ascribed to the vibration bands of hydroxides and adsorbed water molecules, and (ii) at low frequency (600 cm^{-1}) indicative of the Zn–O scaffold [61]. Finally, the ATR-FTIR spectrum of the CMZ-35 nanocomposite (used to prepare the best performing NF membrane in this study, as demonstrated in Section 3.3) showed 4 main signals: (i) a broad band within 3000 and 3600 cm^{-1}, which corresponded to hydroxyls and $–NH_2$ groups on chitosan and MOF, and to the physiosorbed water molecules, (ii) an absorption band at 600 cm^{-1} associated to the presence of ZnO, (iii) a peak at 1639 cm^{-1} distinctive for the vibration of N–H groups and (iv) a final peak 1708 cm^{-1} for O–C–O groups. The positions of these last two peaks, deriving the former from chitosan and the latter from the NH_2-MIL-101(Al), were slightly shifted in the composite when compared to those of the pristine materials, indicating strong interaction between the components of the membrane active layer.

3.2. Characterization of nanocomposite membranes

Fig. 5 shows the SEM micrographs of the surfaces and cross-sections of the original PSF substrate and the CMZ-35 membranes after coating. The commercial PSF substrate presented a smooth surface (Fig. 5a) with the exception of a few valleys, deriving most certainly from the fabrication process. At the same lens enlargement, the surface of the CMZ-35 membrane (Fig. 5b) presented a polycrystalline and rougher surface, evenly distributed with a few exceptions due to the aggregation of some nanoparticles during the deposition of the active layer. This indicated that the selective active layer had been successfully deposited on the PSF substrate during the coating stage. Furthermore, the cross-section morphology of both support and CMZ-35 membrane were analyzed and compared. Fig. 5c shows that the PSF substrate presented an asymmetrical structure with a thin and relatively dense skin at the top and a macroporous finger-like sublayer. The substrate presented an overall thickness of 383 ± 9 μm. As far as the cross section of CMZ-35 was concerned (see Fig. 5d), it was possible to observe a thin dense active layer on top of the PSF substrate with an average thickness equal to 29 ± 4 μm.

To confirm that the top dense thin layer, identified in Fig. 5d, is actually the CMZ-35 active layer, Energy-Dispersive X-ray (EDX) spectroscopy was used. The concentrations of the main elements (i.e., C, S, O, Al and Zn) that comprise (i) the substrate polymer (PSF) and (ii) the selective active layer were determined. As it is possible to observe in Fig. 6, the characteristic elements of CMZ-materials, namely Al and Zn, were found at high concentration in the top layer, confirming that it was indeed the intended selective active layer. As for O, a larger concentration was observed in the active layer due to (i) the presence of ZnO, (ii) the –OH groups and C–O bonds of chitosan, and (iii) the O atoms in the NH_2-MIL101(Al) framework. On the other hand, S and C are clearly located in the area corresponding to the membrane support due to both

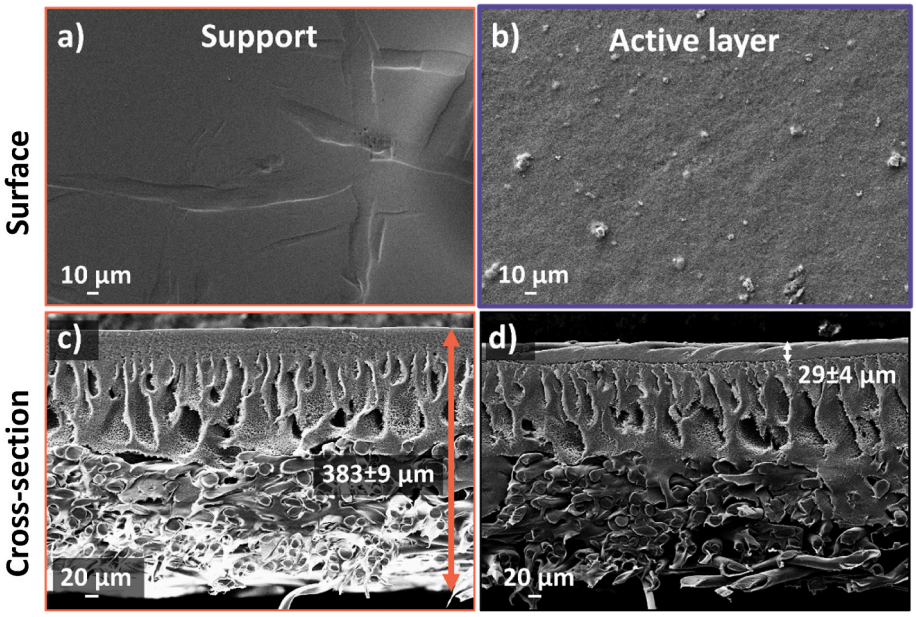

Fig. 5. SEM images of the surfaces (a,b) and the cross-sections (c,d) of the membrane support and active layer (CMZ-35). The orange arrow indicates the support layer thickness; the white arrow indicates the active layer thickness. (For interpretation of the references to colour in this figure legend, the reader is referred to the Web version of this article.)

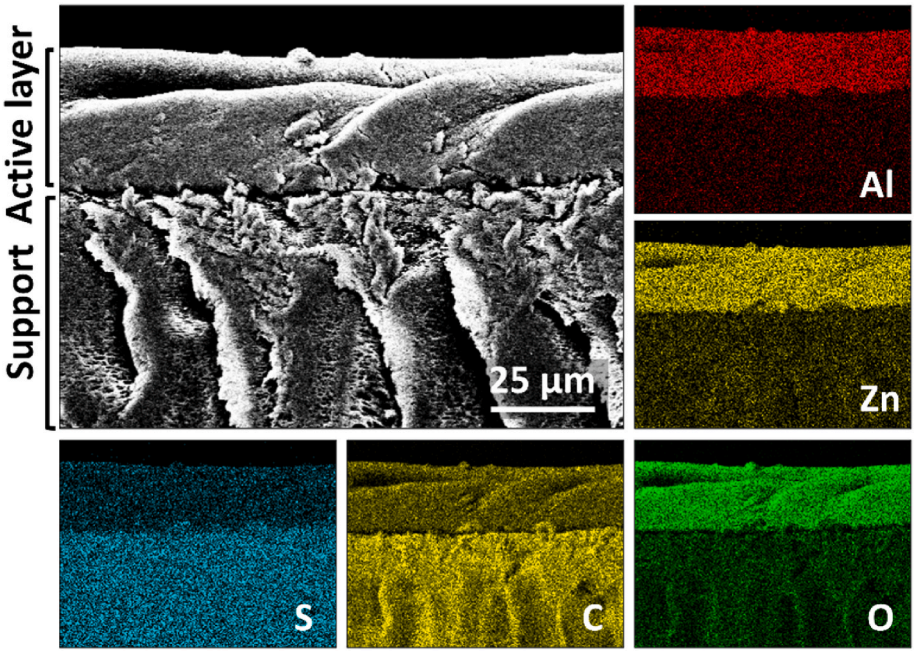

Fig. 6. EDX analysis of the CMZ-35 membrane.

being characteristic elements of the polymer forming the substrate, namely PSF. Moreover, the characteristic elements of MOF and ZnO, which are Al and Zn respectively were evenly distributed in the active layer indicating a good dispersion of the nanoparticles in the chitosan matrix. The concentration of these two elements is negligible outside the area of the micrograph corresponding to the active layer, indicating no relevant infiltration of the CMZ material in the membrane support. The active layer homogeneity was confirmed by the N_2 absorption porosimetry which was performed on the unsupported composite membrane materials. Indeed, upon addition of chitosan, the specific surface area dropped to 42 $m^2\ g^{-1}$ for CMZ-0 and to values smaller than 5 $m^2\ g^{-1}$ for all the other membrane materials (CMZ-20, CMZ-35, CMZ-60, and CMZ-80) The depletion of accessible porosity could be considered as a consequence of the full embedment of the nanoparticles in the continuous chitosan matrix.

In general, an important property to evaluate for NF membranes is their hydrophilicity. It has been previously demonstrated in literature that hydrophilic membranes are resistant to fouling [62]. This is essentially due to the fact that hydrophilic surface groups can either generate strong hydrogen bonds with water molecules or attract them electrostatically. A water boundary layer is consequently formed at the membrane surface, repelling possible foulants. Since the main goal of the current study is to develop a highly selective NF membrane for magnesium and calcium recovery from seawater and waste brines with organic matter, it is even more important to evaluate the membrane hydrophilicity. More specifically, the effect of ZnO loading on the hydrophilicity of the NF membrane was investigated by measuring the water contact angle of each membrane. Fig. 7a depicts the water contact angle measured for the uncoated PSF substrate and the NF membranes characterized by different ZnO loading at a fixed time interval of 30 s after the water drop touched the membrane surface. It is worth mentioning that the water contact angle measurements did not undergo distinct changes during the measurement time of the analyses. As it is possible to observe in Fig. 7a, the presence of an active layer (without ZnO) reduced the water contact angle of the PSF substrate from 48.9° ± 3 (PSF) to 37.8° ± 2 (CMZ-0), making it more hydrophilic. This can be ascribed to the presence of amino and hydroxyl groups on the membrane active layer and the higher surface roughness. However, it was further observed that the gradual increase of ZnO within the active layer allowed to reduce even more the water contact angle from 37.8° ± 2 (CMZ-0) to 14.1° ± 1 (CMZ-60). This was due essentially to the high polarity and high abundance of hydroxyl groups in the ZnO nanocrystals

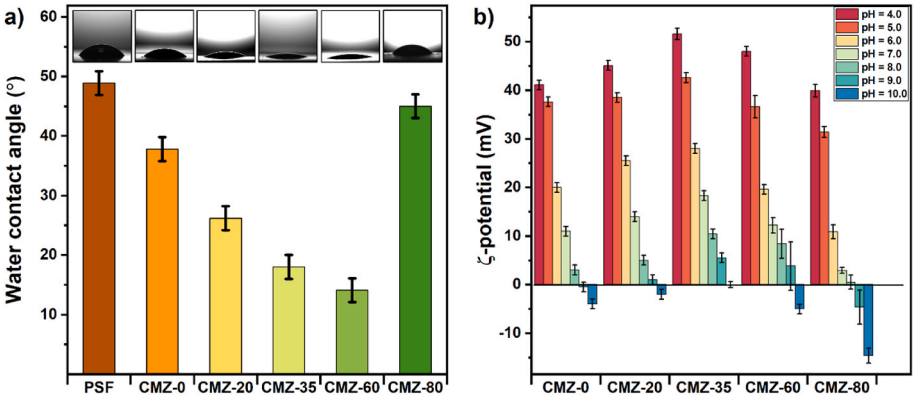

Fig. 7. a) Water contact angle analysis of UF membrane (PSF) and NF membranes of this work; b) ζ-potential of the membrane materials CMZ-0, CMZ-20, CMZ-35, CMZ-60, CMZ-80 as a function of the pH.

[63]. Therefore, it could be deduced that ZnO was the main contributor to the enhancement of surface hydrophilicity and not the MOF, endowing the membrane with a potential anti-fouling capacity. However, in the range of high ZnO loading, two phenomena were observed: (i) the effect of ZnO on the increase of surface hydrophilicity became less dominant, consistent with previous reported works [56,64]; (ii) high ZnO loading without the presence of MOF (CMZ-80) caused the formation of a very defective and unstable active layer, leading therefore to a membrane with a similar behaviour of an ultrafiltration membrane. This was also reflected in its selective performances (see Section 3.3).

Moreover, ZnO is known not only for its hydrophilic properties, but also for its high positive electric charge in aqueous solutions due to the acid-base properties of the surface groups, resulting in a isoelectric point higher than pH 9.0 [63]. The latter property is the most essential to be tuned in the synthesized NF membrane to achieve high selectivity towards Mg^{2+} and Ca^{2+} ions (main target of this work). Nevertheless, CMZ membranes are ternary systems consisting of chitosan, NH_2-functionalized MOF, and ZnO nanoparticles. Therefore, the surface charge of CMZ depend on the type and the density of the functionalities available on the surface of the nanocomposite. For this reason the effect of the composition on the electric surface charge of the CMZ membranes was investigated by measuring the ζ-potential within a wide pH range (from 3.0 to 12.0). Fig. 7b shows that the NF membrane without ZnO (CMZ-0) presented a very high ζ-potential value equal, namely +43 mV, at pH = 3.0 and became negatively charged only at pH values higher than 9. The high positive surface charge of CMZ-0 could be ascribed to the protonated amino groups in the MOF. However, as can be perceived from Fig. 7b, the increase of ZnO loading from 0 (CMZ-0) to 35% (CMZ-35) promoted an increase of electric surface charge of the membrane at any fixed pH value, confirming a strong interaction between the CMZ components. However, once ZnO substituted the MOF as the main component, the increase of ZnO was accompanied by a decrease of ζ-potential at a fixed pH value. Reason for this is that the MOF provides a large density of amino groups, providing high surface charge and facilitating the dispersion of the nanocomposite nanoparticles. When the ZnO nanoparticles became the predominant component in respect to the MOF, the CMZ nanocomposites show an isoelectric point close to that expected for ZnO nanoparticles embedded in chitosan (pKa ~ 6.5) [65,66]. It is also worth noting how the ζ-potential of the novel synthesized membranes always assumed a positive value within the pH range 5 and 8, which corresponded to the relevant pH interval for the tests in this study and for real-life applications. In particular, the ζ-potential of CMZ-35 ranged from 44 mV at pH = 5.0 to 11 mV at pH = 8.0. Furthermore, CMZ-35 presented a neutral surface charge only in very alkaline environments (pH = 10), unlike commercial NF membranes which are usually neutral or negatively charged already at pH = 7 [23].

3.3. Filtration of single salt solutions

The filtration performance of the four different NF membranes characterized by different ZnO loadings was investigated at 5 bar with four different single salt solutions: NaCl (1000 mg L^{-1}), Na_2SO_4 (1000 mg L^{-1}), $MgCl_2$ (1000 mg L^{-1}) and $CaCl_2$ (1000 mg L^{-1}). Results of the salt rejection and water permeability are reported in Fig. 8 with a maximum standard deviation value equal to 5% and 4%, respectively.

As can be observed in Fig. 8a, most of the membranes under investigation (CMZ-0, 20, 35) presented a salt rejection (R) that followed the same order: $MgCl_2$ > $CaCl_2$ > NaCl > Na_2SO_4. Such a trend could be explained by the combination of two effects: (i) steric exclusion and (ii) Donnan exclusion. As concerns the steric effect, Mg^{2+} and Ca^{2+} present larger hydrated and Stokes radii than Na^+, therefore their transport across the membrane is more obstructed when compared to that of Na^+. As for the Donnan effect, given that the NF membranes present a positive surface charge and that Mg^{2+} and Ca^{2+} present a larger charge density than Na^+, the multivalent cations present a higher rejection than Na^+. As far as the counterions are concerned, transmembrane permeation is therefore less hindered. In addition, the counterions that also present a high charge density such as SO_4^{2-} can permeate the most due to the strongest electrostatic attraction. This also explains why the salt rejection of Na_2SO_4 was the lowest for all membranes. Furthermore, it was possible to observe in Fig. 8a that the increase of ZnO loading led to an increase in salt rejection for all salts, reaching the set of highest salt rejections with CMZ-35 (R_{MgCl_2} = 90.1%, R_{CaCl_2} = 86.49%, R_{NaCl} = 32.29%, $R_{Na_2SO_4}$ = 18.28%). The increase of salt rejections from CMZ-0 to CMZ-35 was due to two phenomena related to the higher concentration of ZnO: (i) an increase in the positive surface charge of the membrane (as demonstrated in Fig. 7b) and (ii) aggregation of the nanopowder making the active layer denser and therefore reducing the membrane pore size. As a matter of fact, the addition of ZnO within the active layer reduced the specific area of the membrane from 42 m^2/g (CMZ-0) to 4 m^2/g (CMZ-35). However, from CMZ-35 to CMZ-80, it was possible to witness a decrease in the salt rejection performance. This opposite trend can be ascribed to the high ZnO concentrations. More specifically, as also reported in literature [64], when the concentration of ZnO is too high, nanoaggregates are formed. This leads to (i) a decrease of ζ-potential (as reported in Section 3.2), compromising the homogeneity and the mechanical integrity of the consolidated active layer film. Such features had led in fact to fractures in the thin film membrane active layer, confirmed via SEM analysis (see Fig. 9), thus reducing its rejection performances.

It is also to be noted that both the ζ-potential reduction and the fractures were most likely to be the causes of the salt rejection order variation of CMZ-60 too (i.e. $R_{CaCl_2} > R_{MgCl_2} > R_{NaCl} > R_{Na_2SO_4}$), where the electric expulsion effect would influence less than in the previous cases. Furthermore, due to the high defect density in the active layer, as previously mentioned in Section 3.2, CMZ-80 behaved similar to an

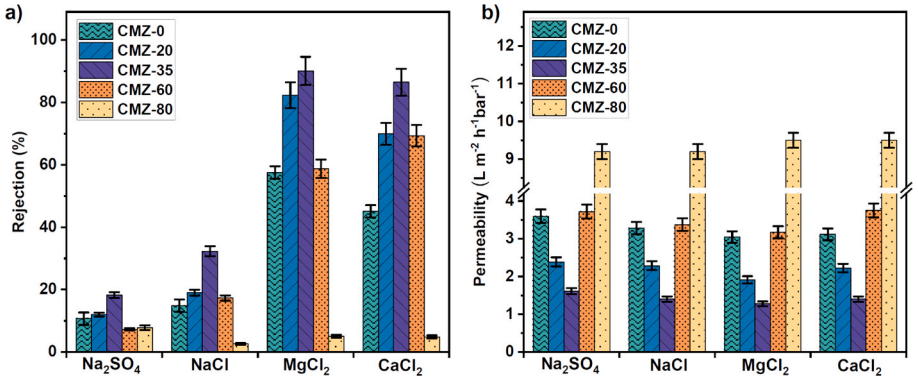

Fig. 8. a) Salt rejections and b) permeabilities of the tested NF membranes for single salt solution feed at 1000 mg L^{-1} and at 5 bar.

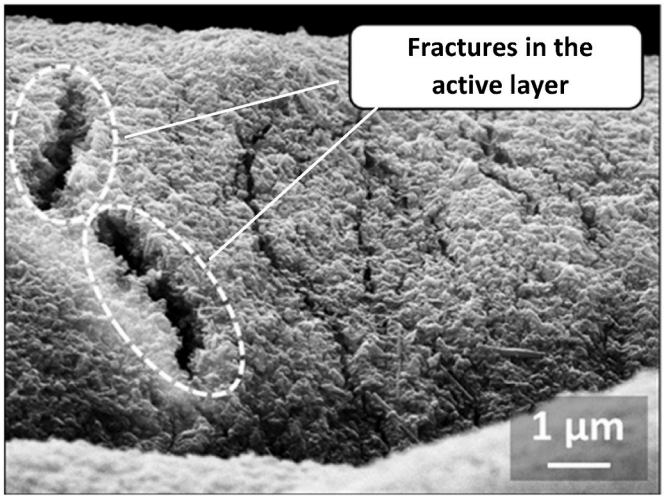

Fig. 9. Post-mortem SEM image of the active layer of CMZ-60. Microfractures (circled) are present due to the aggregation of ZnO nanoparticles.

ultrafiltration membrane, presenting low rejection values for all salts. Fig. 8b reports the trend of membrane permeability for the four different ZnO loadings. As it is possible to observe, whilst the salt rejection trend presented a maximum point with CMZ-35, the permeability trend presented a minimum value in correspondence to CMZ-35: it is equal to 1.5 L m^{-2} h^{-1} bar^{-1} on average, i.e., within the typical range of permeability values of commercial NF membranes [67]. This result is surprising, considering that the active layer of this membrane presents a thickness of 29±4 µm. Indeed, these results indicate that CMZ materials present specific permeabilities greater than 40 L m^{-2} h^{-1} bar^{-1} µm, i.e., superior to all the commercial NF membranes and novel MOF-based membranes which are typically much thinner [68]. Attempts to reduce the active layer thickness were made by diluting the coating dispersion but homogenous coating was very much challenging resulting in membranes with poor selectivity.

Overall, the best performing membrane, namely CMZ-35, proved to present a high selectivity towards multivalent cations such as Mg^{2+} and Ca^{2+} and high permeation of SO_4^{2-}. Subsequently, such selectivity was compared to that of commercial NF membranes and novel positively charged NF membranes recently presented in literature, at operating conditions similar to those of the current study. As can be observed in Fig. 10a–d, CMZ-35 was able to fall in the region of interest (high selectivity towards $MgCl_2$ and $CaCl_2$), unlike all the other membranes taken into consideration, thus demonstrating to be currently the best NF membrane with the requested properties in question. As a matter of fact, a few NF membranes such as the commercial NF90 [27,31,32,36,69] present high rejection for all salts. NF270, on the other hand, which is a looser NF membrane than NF90 and presents a negative surface charge [70], shows high rejections towards sulphates, being negatively charge. NF270 was found, in fact, to be in the opposite region to that of interest of this study. Furthermore, other recently proposed NF membranes presented instead relatively low rejections for all salts such as [28,39].

3.4. Filtration of real seawater and desalination brine

The ionic selectivities (*IS*) of CMZ-35 were also investigated in real application scenarios, tested at 30 bar and cross-flow velocity of 3.5 L/min with synthetic seawater and desalination brine solutions.

CMZ-35 results of *IS* were then compared to those of two commercial NF membranes (NF90, NF270), as shown in Fig. 11. It is worth mentioning that in the case of seawater treatment, for most cases, the

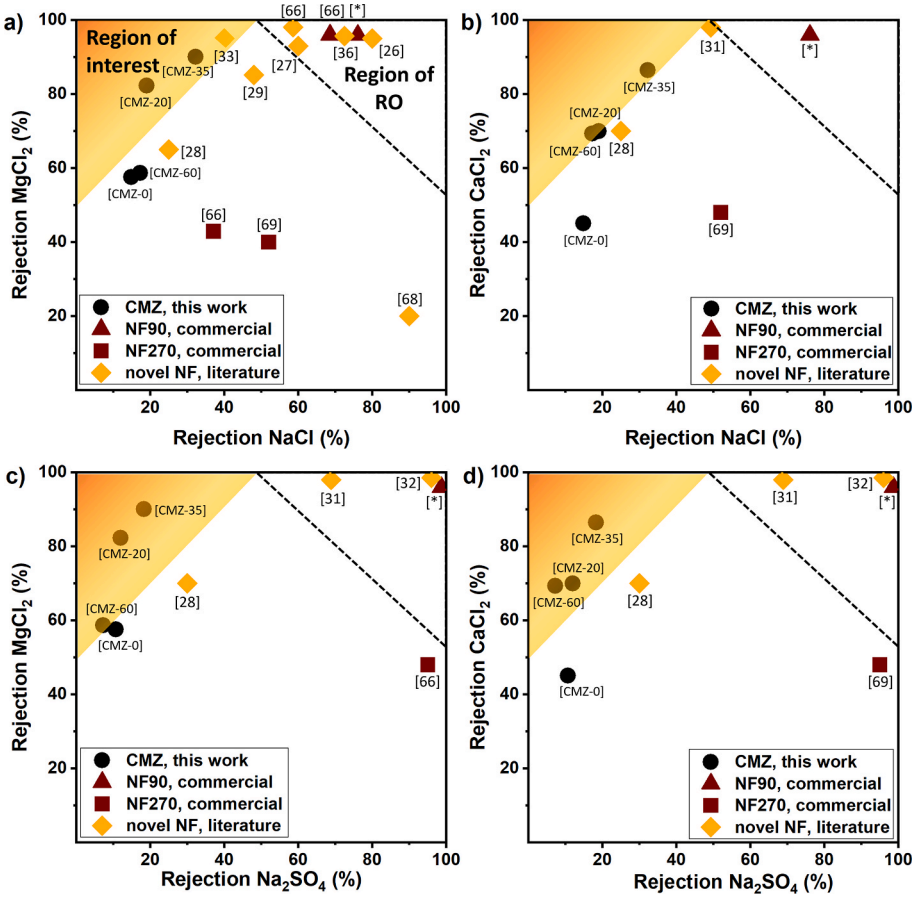

Fig. 10. Rejections for CMZ membranes of this work, commercial NF membranes, and positively charged NF membranes in literature ([26–29,31–33,36,69,71,72]) for the salt couples: (a) $MgCl_2$/NaCl, (b) $CaCl_2$/NaCl, (c) $MgCl_2$/Na_2SO_4, and (d) $CaCl_2$/Na_2SO_4 at operating pressures reported in Table 1. Region of interest: high rejection values towards $MgCl_2$ and $CaCl_2$ respect to NaCl and Na_2SO_4; Region of RO: typical rejection values for RO membranes. *Tested in this work.

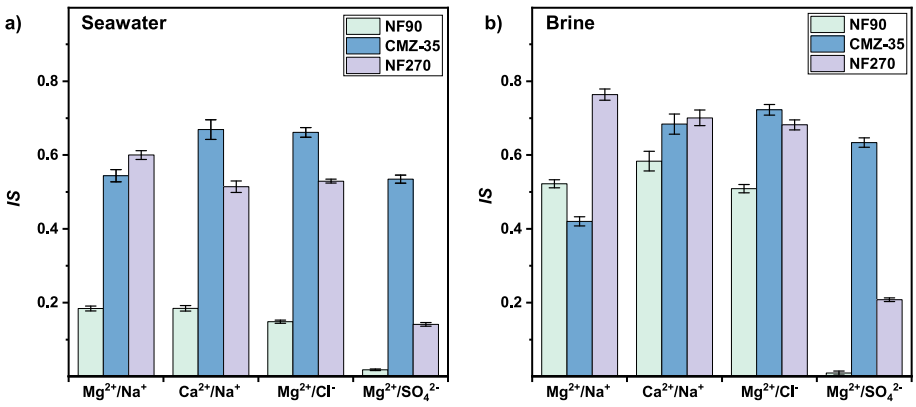

Fig. 11. Ion Selectivities (*IS,* calculated according to equation (3)) of CMZ-35 and the commercial membranes NF90 and NF270 in the treatment of (a) seawater and (b) brine.

selectivity towards multivalent cations with respect to mono/multivalent anions was successfully higher for CMZ-35 when compared to the two commercial NF membranes. Exceptions in which CMZ-35 presented an intermediate selectivity between that of NF90 and NF270 were Mg^{2+}/Na^{+} and Ca^{2+}/SO_4^{2-}. Reasons of such behaviour are to be essentially associated with the maintenance of a positive surface charge of the novel NF membrane within slightly alkaline environments (i.e. seawater or brine), unlike NF90 and NF270. As far as the desalination brine scenario is concerned, the high ionic concentration of the feed solution led to a greater reduction of monovalent ion rejection than that of multivalent rejections. This resulted in an overall higher ionic selectivity for each membrane for brine treatment when compared to the scenario of seawater. In the scenario of brine, CMZ-35 also presented higher ionic selectivity values for most cases than NF90 and NF270. However, apart from the usual exceptions concerning Mg^{2+}/Na^{+} and Ca^{2+}/SO_4^{2-}, CMZ-35 also presented lower selectivity values for Ca^{2+}/Na^{+} than NF270. Anyhow, when brine was treated, CMZ-35 proved to be still competitive with common commercial NF membranes that are widely used at industrial scale.

4. Conclusions

To enhance valuable multivalent-cations recovery within ZLD/MLD systems from seawater/desalination brine, a novel positively charged NF membrane was synthesized. More specifically, magnesium and calcium were the main ions to be purposely recovered, being magnesium a CRM and calcium a major component in seawater/brine that can be employed in several industrial applications. To such an end, components of the novel NF membrane were carefully selected to promote a highly positive surface charge of the NF membrane in alkaline environments, thus selectively rejecting magnesium and calcium. The NF membrane comprised: (i) a microporous asymmetric UF-membrane-like substrate guaranteeing mechanical strength and (ii) a selective active layer of MOF "NH_2-MIL-101(Al)" and ZnO within a chitosan matrix. The nanoparticles comprising the active layer were characterized via SEM, FTIR, DLS and BET, meanwhile morphology, hydrophilicity and electric surface charge were also analyzed for the nanocomposites. The effect of different loadings of MOF and ZnO within the active layer on the selective/permeation performances of the NF membrane was investigated. Results of characterization analyses and initial filtration tests at 5 bar with 1000 mg L^{-1} single salt solutions (NaCl, Na_2SO_4, $MgCl_2$, $CaCl_2$) showed:

(i) The increase of ZnO content within the active layer increased the hydrophilicity and zeta potential of the membrane, promoting higher rejections towards multivalent cations;
(ii) Too high ZnO concentrations caused the phenomenon of pore blockage and microfractures of the active layer, thus reducing all ionic rejections;
(iii) The NF membrane with the highest rejections of $MgCl_2$ (90.10%) and $CaCl_2$ (86.49%) was CMZ-35 (20%wt Chitosan, 35%wt ZnO and 45%wt MOF).

Selectivity properties of the synthesized NF membrane were then compared to those of (i) common commercial NF membranes and (ii) novel positively charged NF membranes reported in literature at the same operating conditions. Results highlighted that CMZ-35 does have the highest selectivity towards $MgCl_2$ and $CaCl_2$ among all the membranes.

Moreover, unlike all the novel positively charged NF membranes introduced in literature, the performances of the novel synthesized membrane of this work were further investigated in real application scenarios. CMZ-35 was tested with synthetic seawater and desalination brine at 30 bar. The achieved ion selectivity values were compared with those of two commercial membranes (NF90, NF270) at the same operating conditions. Results showed that CMZ-35 successfully presented higher Mg^{2+} and Ca^{2+} selectivity than NF90 for seawater treatment and higher values in most cases than NF270. Meanwhile, as far as desalination brine treatment was concerned, similar successful results were also achieved. In conclusion, results demonstrate that CMZ-35, with its low-cost fabrication materials (0.4 €/cm^2 for CMZ-35 vs. 1.2 €/cm^2 for NF90/NF270 [73]) and simple fabrication procedure that does not involve hazardous organic solvents, is currently an intriguing competitive alternative to commercial NF membranes, that could considerably enhance mineral recovery in ZLD/MLD systems for seawater and brine valorization.

Author statement

C. Morgante: Conceptualization, Methodology, Investigation, Data Curation, Writing - Original Draft; **X. Ma:** Investigation, Data Curation; **X. Chen:** Investigation, Data Curation; **D. Wang:** Investigation, Data Curation; **V. Boffa:** Conceptualization, Methodology, Supervision, Writing - Review & Editing; **V. Stathopoulos:** Investigation, Resources, Data Curation, Writing - Review & Editing. **J. Lopez:** Investigation, Data Curation; **J.L. Cortina:** Resources, Supervision, Writing - Review & Editing; **A. Cipollina:** Supervision, Funding acquisition, Data Curation, Writing - Review & Editing; **A. Tamburini:** Supervision, Funding acquisition, Data Curation, Writing - Review & Editing; **G. Micale:** Supervision, Funding acquisition, Data Curation, Writing - Review & Editing.

Declaration of competing interest

The authors declare that they have no known competing financial interests or personal relationships that could have appeared to influence the work reported in this paper.

Data availability

Data will be made available on request.

Acknowledgments

The authors would like to acknowledge that parts of the research activities were carried out within the framework of "Programma Operativo Nazionale Ricerca e Innovazione2014-2020 (CCI 2014IT16M2OP005), Fondo Sociale Europeo, Azione I.1 "Dottorati Innovativi con caratterizzazione Industriale", Code: DOT204NJ79, CUP: B73D20005110001. J. López research was developed under the Margarita Salas postdoctoral fellowship from Ministerio de Universidades (MIU) and founded by the European Union-NextGenerationEU. Moreover, J.L. Cortina received support for the research through the "ICREA Academia" recognition for excellence in research funded by the Generalitat de Catalunya.

Abbreviations

CMZ	Chitosan Metal organic framework Zinc oxide
CRM	Critical Raw Material
DADMAC	Diallyl Dimethyl Ammonium Chloride
DLS	Dynamic Light Scattering
ECH	Epichlorohydrin
EDX	Energy-dispersive X-ray
FE-SEM	Field Emission Scanning Electron Microscopy
FTIR	Fourier-Transform Infrared spectroscopy
HACC	2-hydroxypropyltrimethyl Ammonium Chloride Chitosan
HPLC	High-Performance Liquid Chromatography
MLD	Minimal Liquid Discharge
MO	Metal Oxide
MOF	Metal Organic Framework
NF	Nanofiltration
PAI	Polyamide–imide
PAMAM	Poly(amidoamine)
PAN	Polyacrylonitrile
PDA	Polydopamine
PDMAEMA	Poly (N,N-dimethylaminoethyl methacrylate)
PEI	Polyethylenimine
PEKC	Poly(ether ether ketone)
PES	Polyethersulfone
PIP	Piperazine
PSF	Polysulfone
PVC	Polyvinyl Chloride
RO	Reverse Osmosis
TMC	Trimesoyl Chloride
XRD	X-Ray Diffraction
ZLD	Zero Liquid Discharge

References

[1] European Commission, Critical Raw Materials, 2020, pp. 1–4. https://single-market-economy.ec.europa.eu/sectors/raw-materials/areas-specific-interest/critical-raw-materials_en. (Accessed 10 January 2023).
[2] A. Cipollina, M. Bevacqua, P. Dolcimascolo, A. Tamburini, A. Brucato, H. Glade, L. Buether, G. Micale, Reactive crystallisation process for magnesium recovery from concentrated brines, Desalination Water Treat. 55 (2015) 2377–2388, https://doi.org/10.1080/19443994.2014.947771.
[3] European Commission, Circular Economy Action Plan, 2021. https://ec.europa.eu/environment/strategy/circular-economy-action-plan_en.
[4] X. Zhang, W. Zhao, Y. Zhang, V. Jegatheesan, A review of resource recovery from seawater desalination brine, Rev. Environ. Sci. Biotechnol. 20 (2021) 333–361, https://doi.org/10.1007/s11157-021-09570-4.
[5] P. Dorji, D.I. Kim, S. Hong, S. Phuntsho, H.K. Shon, Pilot-scale membrane capacitive deionisation for effective bromide removal and high water recovery in seawater desalination, Desalination 479 (2020), https://doi.org/10.1016/j.desal.2020.114309.
[6] H. Ohya, T. Suzuki, S. Nakao, Integrated system for complete usage of components in seawater: a proposal of inorganic chemical combinat in seawater, Desalination 134 (2001) 29–36, https://doi.org/10.1016/S0011-9164(01)00112-6.
[7] E. Jones, M. Qadir, M.T.H. van Vliet, V. Smakhtin, S. mu Kang, The state of desalination and brine production: a global outlook, Sci. Total Environ. 657 (2019) 1343–1356, https://doi.org/10.1016/j.scitotenv.2018.12.076.
[8] S. Lattemann, T. Höpner, Environmental impact and impact assessment of seawater desalination, Desalination 220 (2008) 1–15, https://doi.org/10.1016/j.desal.2007.03.009.
[9] T. Jeppesen, L. Shu, G. Keir, V. Jegatheesan, Metal recovery from reverse osmosis concentrate, J. Clean. Prod. 17 (2009) 703–707, https://doi.org/10.1016/j.jclepro.2008.11.013.
[10] G. Cipolletta, N. Lancioni, Ç. Akyol, A.L. Eusebi, F. Fatone, Brine treatment technologies towards minimum/zero liquid discharge and resource recovery: state of the art and techno-economic assessment, J. Environ. Manag. 300 (2021), 113681, https://doi.org/10.1016/j.jenvman.2021.113681.
[11] Z. Wang, A. Deshmukh, Y. Du, M. Elimelech, Minimal and zero liquid discharge with reverse osmosis using low-salt-rejection membranes, Water Res. 170 (2020), 115317, https://doi.org/10.1016/j.watres.2019.115317.
[12] N. Hilal, H. Al-Zoubi, N.A. Darwish, A.W. Mohammad, M. Abu Arabi, A comprehensive review of nanofiltration membranes: treatment, pretreatment, modelling, and atomic force microscopy, Desalination 170 (2004) 281–308, https://doi.org/10.1016/j.desal.2004.01.007.
[13] H. Zhang, Q. He, J. Luo, Y. Wan, S.B. Darling, Sharpening nanofiltration: strategies for enhanced membrane selectivity, ACS Appl. Mater. Interfaces 12 (2020) 39948–39966, https://doi.org/10.1021/acsami.0c11136.
[14] Y. Roy, D.M. Warsinger, J.H. Lienhard, Effect of temperature on ion transport in nanofiltration membranes: diffusion, convection and electromigration, Desalination 420 (2017) 241–257, https://doi.org/10.1016/j.desal.2017.07.020.
[15] K. Gu, S. Wang, Y. Li, X. Zhao, Y. Zhou, C. Gao, A facile preparation of positively charged composite nanofiltration membrane with high selectivity and permeability, J. Membr. Sci. 581 (2019) 214–223, https://doi.org/10.1016/j.memsci.2019.03.057.
[16] M. Figueira, D. Rodríguez-Jiménez, J. López, M. Reig, J.L. Cortina, C. Valderrama, Experimental and economic evaluation of nanofiltration as a pre-treatment for added-value elements recovery from seawater desalination brines, Desalination 549 (2023), https://doi.org/10.1016/j.desal.2022.116321.
[17] Sea4Value Project (n.d.) 1–7, https://sea4value.eu/. (Accessed 10 January 2023).
[18] M. Reig, S. Casas, O. Gibert, C. Valderrama, J.L. Cortina, Integration of nanofiltration and bipolar electrodialysis for valorization of seawater desalination brines: production of drinking and waste water treatment chemicals, Desalination 382 (2016) 13–20, https://doi.org/10.1016/j.desal.2015.12.013.
[19] M.E.A. Ali, Nanofiltration process for enhanced treatment of RO brine discharge, Membranes 11 (2021) 212, https://doi.org/10.3390/membranes11030212.
[20] C. Morgante, F. Vassallo, D. Xevgenos, A. Cipollina, M. Micari, A. Tamburini, G. Micale, Valorisation of SWRO brines in a remote island through a circular approach: techno-economic analysis and perspectives, Desalination (2022) 542, https://doi.org/10.1016/j.desal.2022.116005.
[21] Zero Brine Project (2020) 10–12.
[22] F. Du, D.M. Warsinger, T.I. Urmi, G.P. Thiel, A. Kumar, J.H. Lienhard, Sodium hydroxide production from seawater desalination brine: process design and energy efficiency, Environ. Sci. Technol. 52 (2018) 5949–5958, https://doi.org/10.1021/acs.est.8b01195.
[23] S. Cheng, D.L. Oatley, P.M. Williams, C.J. Wright, Characterisation and application of a novel positively charged nanofiltration membrane for the treatment of textile industry wastewaters, Water Res. 46 (2012) 33–42, https://doi.org/10.1016/j.watres.2011.10.011.
[24] C. Bellona, J.E. Drewes, The role of membrane surface charge and solute physico-chemical properties in the rejection of organic acids by NF membranes, J. Membr. Sci. 249 (2005) 227–234, https://doi.org/10.1016/j.memsci.2004.09.041.
[25] A.E. Yaroshchuk, Non-steric mechanism of nanofiltration: superposition of donnan and dielectric exclusion, Sep. Purif. Technol. (2001) 143–158, https://doi.org/10.1016/S1383-5866(00)00159-3, 22–23.
[26] D. Wu, Y. Huang, S. Yu, D. Lawless, X. Feng, Thin film composite nanofiltration membranes assembled layer-by-layer via interfacial polymerization from polyethylenimine and trimesoyl chloride, J. Membr. Sci. 472 (2014) 141–153, https://doi.org/10.1016/j.memsci.2014.08.055.
[27] C. Feng, J. Xu, M. Li, Y. Tang, C. Gao, Studies on a novel nanofiltration membrane prepared by cross-linking of polyethyleneimine on polyacrylonitrile substrate, J. Membr. Sci. 451 (2014) 103–110, https://doi.org/10.1016/j.memsci.2013.10.003.
[28] X.L. Li, L.P. Zhu, J.H. Jiang, Z. Yi, B.K. Zhu, Y.Y. Xu, Hydrophilic nanofiltration membranes with self-polymerized and strongly-adhered polydopamine as separating layer, Chinese J. Polym. Sci. (English Ed. 30 (2012) 152–163, https://doi.org/10.1007/s10118-012-1107-5.
[29] Y.C. Xu, Z.X. Wang, X.Q. Cheng, Y.C. Xiao, L. Shao, Positively charged nanofiltration membranes via economically mussel-substance-simulated co-deposition for textile wastewater treatment, Chem. Eng. J. 303 (2016) 555–564, https://doi.org/10.1016/j.cej.2016.06.024.

[30] F. Liu, B.R. Ma, D. Zhou, L.J. Zhu, Y.Y. Fu, L.X. Xue, Positively charged loose nanofiltration membrane grafted by diallyl dimethyl ammonium chloride (DADMAC) via UV for salt and dye removal, React. Funct. Polym. 86 (2015) 191–198, https://doi.org/10.1016/j.reactfunctpolym.2014.09.003.
[31] H.Z. Zhang, Z.L. Xu, H. Ding, Y.J. Tang, Positively charged capillary nanofiltration membrane with high rejection for Mg2 + and Ca2 + and good separation for Mg2 + and Li +, Desalination 420 (2017) 158–166, https://doi.org/10.1016/j.desal.2017.07.011.
[32] C. Wu, S. Liu, Z. Wang, J. Zhang, X. Wang, X. Lu, Y. Jia, W.S. Hung, K.R. Lee, Nanofiltration membranes with dually charged composite layer exhibiting super-high multivalent-salt rejection, J. Membr. Sci. 517 (2016) 64–72, https://doi.org/10.1016/j.memsci.2016.05.033.
[33] W. Fang, L. Shi, R. Wang, Interfacially polymerized composite nanofiltration hollow fiber membranes for low-pressure water softening, J. Membr. Sci. 430 (2013) 129–139, https://doi.org/10.1016/j.memsci.2012.12.011.
[34] H. Deng, Y. Xu, Q. Chen, X. Wei, B. Zhu, High flux positively charged nanofiltration membranes prepared by UV-initiated graft polymerization of methacrylatoethyl trimethyl ammonium chloride (DMC) onto polysulfone membranes, J. Membr. Sci. 366 (2011) 363–372, https://doi.org/10.1016/j.memsci.2010.10.029.
[35] R. Huang, G. Chen, M. Sun, Y. Hu, C. Gao, Studies on nanofiltration membrane formed by diisocyanate cross-linking of quaternized chitosan on poly(acrylonitrile) (PAN) support, J. Membr. Sci. 286 (2006) 237–244, https://doi.org/10.1016/j.memsci.2006.09.045.
[36] L. Lianchao, W. Baoguo, T. Huimin, C. Tianlu, X. Jiping, A novel nanofiltration membrane prepared with PAMAM and TMC by in situ interfacial polymerization on PEK-C ultrafiltration membrane, J. Membr. Sci. 269 (2006) 84–93, https://doi.org/10.1016/j.memsci.2005.06.021.
[37] R. Du, J. Zhao, Properties of poly (N,N-dimethylaminoethyl methacrylate)/polysulfone positively charged composite nanofiltration membrane, J. Membr. Sci. 239 (2004) 183–188, https://doi.org/10.1016/j.memsci.2004.03.029.
[38] X.H. Ma, Z. Yang, Z.K. Yao, Z.L. Xu, C.Y. Tang, A facile preparation of novel positively charged MOF/chitosan nanofiltration membranes, J. Membr. Sci. 525 (2017) 269–276, https://doi.org/10.1016/j.memsci.2016.11.015.
[39] J. Ma, Y. Ying, X. Guo, H. Huang, D. Liu, C. Zhong, Fabrication of mixed-matrix membrane containing metal-organic framework composite with task-specific ionic liquid for efficient CO2 separation, J. Mater. Chem. A. 4 (2016) 7281–7288, https://doi.org/10.1039/c6ta02611g.
[40] L. Zhu, H. Yu, H. Zhang, J. Shen, L. Xue, C. Gao, B. Van Der Bruggen, Mixed matrix membranes containing MIL-53(Al) for potential application in organic solvent nanofiltration, RSC Adv. 5 (2015) 73068–73076, https://doi.org/10.1039/c5ra10259f.
[41] S. Mohammad Nejad, S.F. Seyedpour, S. Aghapour Aktij, M. Dadashi Firouzjaei, M. Elliott, A. Tiraferri, M. Sadrzadeh, A. Rahimpour, Loose nanofiltration membranes functionalized with in situ-synthesized metal organic framework for water treatment, Mater. Today Chem. 24 (2022), https://doi.org/10.1016/j.mtchem.2022.100909.
[42] H. Liu, M. Zhang, H. Zhao, Y. Jiang, G. Liu, J. Gao, Enhanced dispersibility of metal-organic frameworks (mofs) in the organic phase: via surface modification for tfn nanofiltration membrane preparation, RSC Adv. 10 (2020) 4045–4057, https://doi.org/10.1039/c9ra09672h.
[43] R.-H. Huang, G.-H. Chen, M.-K. Sun, C.-J. Gao, Hexamethylene diisocyanate crosslinking 2-Hydroxypropyltrimethyl ammonium chlroide chitosan/poly (acrylonitrile) composite, J. Appl. Toxicol. 13 (1993) 435–439, https://doi.org/10.1002/jat.2550130611.
[44] D.L. Zhao, S. Japip, Y. Zhang, M. Weber, C. Maletzko, T.-S. Chung, Emerging thin-film nanocomposite (TFN) membranes for reverse osmosis: a review, Water Res. (2020), https://doi.org/10.1016/j.watres.2020.115557.
[45] Z. Yang, H. Guo, Z.K. Yao, Y. Mei, C.Y. Tang, Hydrophilic silver nanoparticles induce selective nanochannels in thin film nanocomposite polyamide membranes, Environ. Sci. Technol. 53 (2019) 5301–5308, https://doi.org/10.1021/acs.est.9b00473.
[46] W.J. Lau, S. Gray, T. Matsuura, D. Emadzadeh, J.P. Chen, A.F. Ismail, A Review on Polyamide Thin Film Nanocomposite (TFN) Membranes: History, Applications, Challenges and Approaches, 2015, https://doi.org/10.1016/j.watres.2015.04.037. This.
[47] B. Khorshidi, I. Biswas, T. Ghosh, T. Thundat, M. Sadrzadeh, Robust fabrication of thin film polyamide-TiO2 nanocomposite membranes with enhanced thermal stability and anti-biofouling propensity, Sci. Rep. 8 (2018), https://doi.org/10.1038/s41598-017-18724-w.
[48] M. Ben-Sasson, X. Lu, E. Bar-Zeev, K.R. Zodrow, S. Nejati, G. Qi, E.P. Giannelis, M. Elimelech, In situ formation of silver nanoparticles on thin-film composite reverse osmosis membranes for biofouling mitigation, Water Res. 62 (2014) 260–270, https://doi.org/10.1016/j.watres.2014.05.049.
[49] L. Shen, Z. Huang, Y. Liu, R. Li, Y. Xu, G. Jakaj, H. Lin, Polymeric membranes incorporated with ZnO nanoparticles for membrane fouling mitigation: a brief review, Front. Chem. 8 (2020), https://doi.org/10.3389/fchem.2020.00224.
[50] M. Sheikh, M. Pazirofteh, M. Dehghani, M. Asghari, M. Rezakazemi, C. Valderrama, J.L. Cortina, Application of ZnO nanostructures in ceramic and polymeric membranes for water and wastewater technologies: a review, Chem. Eng. J. 391 (2020), https://doi.org/10.1016/j.cej.2019.123475.
[51] P. Kanmani, J.W. Rhim, Properties and characterization of bionanocomposite films prepared with various biopolymers and ZnO nanoparticles, Carbohydr. Polym. 106 (2014) 190–199, https://doi.org/10.1016/j.carbpol.2014.02.007.
[52] M. Zare, K. Namratha, S. Ilyas, A. Sultana, A. Hezam, L. Sunil, M.A. Surmeneva, R. A. Surmenev, M.B. Nayan, S. Ramakrishna, S. Mathur, K. Byrappa, Emerging trends for ZnO nanoparticles and their applications in food packaging, ACS Food Sci. Technol. (2022), https://doi.org/10.1021/acsfoodscitech.2c00043.
[53] P. Serra-Crespo, E.V. Ramos-Fernandez, J. Gascon, F. Kapteijn, Synthesis and characterization of an amino functionalized MIL-101(Al): separation and catalytic properties, Chem. Mater. 23 (2011) 2565–2572, https://doi.org/10.1021/cm103644b.
[54] T. Wittmann, R. Siegel, N. Reimer, W. Milius, N. Stock, J. Senker, Enhancing the water stability of Al-MIL-101-NH2 via postsynthetic modification, Chem. Eur J. 21 (2015) 314–323, https://doi.org/10.1002/chem.201404654.
[55] B.E. Warren, X-Ray Diffraction, Addison-Wesley Publishing Co., 1969.
[56] S. Balta, A. Sotto, P. Luis, L. Benea, B. Van der Bruggen, J. Kim, A new outlook on membrane enhancement with nanoparticles: the alternative of ZnO, J. Membr. Sci. 389 (2012) 155–161, https://doi.org/10.1016/j.memsci.2011.10.025.
[57] M. Purushothaman, V. Arvind, K. Saikia, V.K. Vaidyanathan, Fabrication of highly permeable and anti-fouling performance of Poly(ether ether sulfone) nanofiltration membranes modified with zinc oxide nanoparticles, Chemosphere (2022) 286, https://doi.org/10.1016/j.chemosphere.2021.131616.
[58] B. Seoane, C. Téllez, J. Coronas, C. Staudt, NH2-MIL-53(Al) and NH2-MIL-101(Al) in sulfur-containing copolyimide mixed matrix membranes for gas separation, Sep. Purif. Technol. 111 (2013) 72–81, https://doi.org/10.1016/j.seppur.2013.03.034.
[59] M. Hartmann, M. Fischer, Amino-functionalized basic catalysts with MIL-101 structure, Microporous Mesoporous Mater. 164 (2012) 38–43, https://doi.org/10.1016/j.micromeso.2012.06.044.
[60] R. Chang, J. Ma, J. Wang, Y. Liu, X. Guo, H. Qu, Efficient adsorption of dyes using polyethyleneimine-modified NH2-MIL-101(Al) and its sustainable application as a flame retardant for an epoxy resin, ACS Omega 5 (2020) 32286–32294, https://doi.org/10.1021/acsomega.0c04118.
[61] S.O.B. Oppong, W.W. Anku, F. Opoku, S.K. Shukla, P.P. Govender, Photodegradation of eosin yellow dye in water under simulated solar light irradiation using La–doped ZnO nanostructure decorated on graphene oxide as an advanced photocatalyst, ChemistrySelect 3 (2018) 1180–1188, https://doi.org/10.1002/slct.201702470.
[62] E. Virga, K. Žvab, W.M. de Vos, Fouling of nanofiltration membranes based on polyelectrolyte multilayers: the effect of a zwitterionic final layer, J. Membr. Sci. 620 (2021), https://doi.org/10.1016/j.memsci.2020.118793.
[63] C. Ursino, R. Castro-Muñoz, E. Drioli, L. Gzara, M.H. Albeirutty, A. Figoli, Progress of nanocomposite membranes for water treatment, Membranes 8 (2018) 1–40, https://doi.org/10.3390/membranes8020018.
[64] T. Kusworo, R.E. Nugraheni, N. Aryanti, The effect of membrane modification using TiO 2 , ZnO, and GO nanoparticles: challenges and future direction in wastewater treatment, IOP Conf. Ser. Mater. Sci. Eng. 1053 (2021), 012135, https://doi.org/10.1088/1757-899x/1053/1/012135.
[65] G.A. Dakroury, E.A.A. El-Shazly, H.S. Hassan, Preparation and characterization of ZnO/Chitosan nanocomposite for Cs (I) and Sr (II) sorption from aqueous solutions, J. Radioanal. Nucl. Chem. 330 (2021) 159–174, https://doi.org/10.1007/s10967-021-07935-1.
[66] A. Domard, pH and c.d. measurements on a fully deacetylated chitosan: application to CuII—polymer interactions, Int. J. Biol. Macromol. 9 (1987) 98–104.
[67] B. Thabo, B.J. Okoli, S.J. Modise, S. Nelana, Rejection capacity of nanofiltration membranes for nickel, copper, silver and palladium at various oxidation states, Membranes 11 (2021), https://doi.org/10.3390/membranes11090653.
[68] S. Cong, Y. Yuan, J. Wang, Z. Wang, F. Kapteijn, X. Liu, Highly water-permeable metal–organic framework MOF-303 membranes for desalination, J. Am. Chem. Soc. 143 (2021) 20055–20058, https://doi.org/10.1021/jacs.1c10192.
[69] C. Liu, L. Shi, R. Wang, Crosslinked layer-by-layer polyelectrolyte nanofiltration hollow fiber membrane for low-pressure water softening with the presence of SO42- in feed water, J. Membr. Sci. 486 (2015) 169–176, https://doi.org/10.1016/j.memsci.2015.03.050.
[70] A. Imbrogno, A. Tiraferri, S. Abbenante, S. Weyand, R. Schwaiger, T. Luxbacher, A. I. Schäfer, Organic fouling control through magnetic ion exchange-nanofiltration (MIEX-NF) in water treatment, J. Membr. Sci. 549 (2018) 474–485, https://doi.org/10.1016/j.memsci.2017.12.041.
[71] Z. He, K. Wang, Y. Liu, T. Zhang, X. Wang, Fabrication of loose nanofiltration membranes with high rejection selectivity between natural organic matter and salts for drinking water treatment, Membranes 12 (2022), https://doi.org/10.3390/membranes12090887.
[72] C. Boo, Y. Wang, I. Zucker, Y. Choo, C.O. Osuji, M. Elimelech, High performance nanofiltration membrane for effective removal of perfluoroalkyl substances at high water recovery, Environ. Sci. Technol. 52 (2018) 7279–7288, https://doi.org/10.1021/acs.est.8b01040.
[73] Sterlitech, (n.d.). doi:10.1007/s13369-018-3096-3.